Application of the physical optics method to estimate the RCS of a fixed-wing UAV

Tran Nghiep[1], Pham Thanh Dong[2*]

[1]Institute of Technology, General Department of Defense Industry, Van Hoi, Dong Ngac, Hanoi, Vietnam;
[2]Faculty of Aerospace Engineering, Le Quy Don Technical University, 236 Hoang Quoc Viet, Nghia Do, Hanoi, Vietnam.
[*]Corresponding author: pham.thanh-dong@lqdtu.edu.vn
Received 17 Mar. 2026; Revised 4 May 2026; Accepted 8 Jun. 2026; Published 25 Aug. 2026.
DOI: https://doi.org/10.54939/1859-1043.j.mst.113.2026.127-134

ABSTRACT

This paper presents a study on the development of a computational model for the radar cross-section (RCS) of a fixed-wing unmanned aerial vehicle (UAV) based on a three-dimensional triangular-mesh representation and the Physical Optics (PO) approximation. The monostatic scattering problem is formulated as a surface integral and discretized over triangular facets of the UAV geometry. The computational algorithm is optimized for parallel processing to reduce computational time across a wide angular domain. The RCS results in both vertical and horizontal planes are presented in polar plots and analyzed in terms of directional scattering characteristics. The results show that the PO model enables rapid estimation of the RCS distribution of fixed-wing UAVs during the preliminary design stage.

Keywords: RCS; Fixed-wing UAV; Physical optics; Electromagnetic scattering; Numerical modeling; Triangular mesh.

1. INTRODUCTION

The rapid development of small-scale civil and military UAVs is creating new types of threats to infrastructure, equipment, and personnel [1-4]. Consequently, specialized radar systems have emerged in recent years to identify these types of drones, necessitating accurate detection and classification capabilities. Many studies investigating radar signal characteristics show that the majority of scientific works focus on multi-rotor aerial vehicles [5-9]; there remains a significant gap regarding small fixed-wing UAVs, which have not been fully surveyed. This is due to the wide dispersion in size and diverse aerodynamic designs (traditional, delta, flying wing, BWB, etc.) of fixed-wing UAVs, which makes constructing mathematical models more difficult.

Radar Cross Section (RCS) [10, 14, 15] is one of the critical parameters characterizing the detectability of an aerial vehicle. For small fixed-wing UAVs, predicting RCS from the design phase is vital for optimizing aerodynamic shape and stealth characteristics. Common RCS calculation methods include the Finite Element Method (FEM), Method of Moments (MoM), Boundary Integral Method, and the Physical Optics (PO) approximation. For targets with dimensions larger than the wavelength and the requirement for fast calculation over a wide angular range, the PO method is a suitable choice due to its advantages in computational speed, relatively uncomplicated mathematical model, and accuracy that meets preliminary design requirements.

Proceeding from security principles, the authors conducted a study to calculate the radar cross-section for a self-developed fixed-wing UAV, the CX24v1, which has a wingspan of 2 m. The objective of the research is to systematically narrow the gap in RCS characteristics, thereby enabling the identification range of other fixed-wing UAVs in the same size class to be determined using the PO method.

While classical approximate methods like PO are well-established and integrated into commercial simulation software (e.g., CST, Ansys HFSS), developing an in-house computational code is essential for the authors' specific workflow; this in-house MATLAB program allows for seamless, automated integration into the multi-disciplinary design and aerodynamic optimization loop of the newly developed CX24v1 UAV without relying on expensive commercial software licenses. The primary contribution of this work is the development of a rapid, customized preliminary assessment tool to systematically narrow the gap in RCS characteristics for self-developed small fixed-wing UAVs.

2. THEORETICAL BACKGROUND

2.1. Coordinate system and angular convention

The coordinate system and angular conventions are established to align with the UAV's aerodynamic configuration: the positive X-axis points forward, the positive Y-axis points to the left wing, and the positive Z-axis points upward. The angles are defined as follows (Figure 1):

Azimuth angle φ: Scanned in the XY plane, from 0° to 360°, with 0° at the positive X-axis and increasing counter-clockwise. Thus, the vertical longitudinal plane XZ corresponds to φ = 0° (or 180°), and the vertical lateral plane YZ corresponds to φ = 90 ° (or 270 °).

Elevation (pitch) angle θ: In the vertical plane XZ, from 0° to 180°, with 0° at the positive Z-axis, 90° at the positive X-axis, and 180° at the negative Z-axis. Here, the horizontal plane XY corresponds to θ = 90 °.

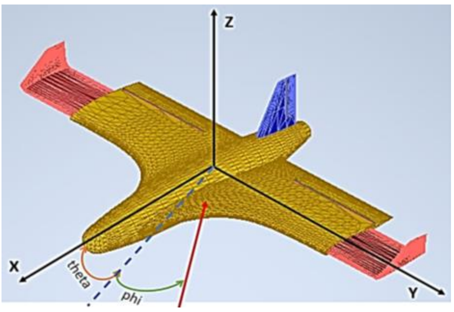

Figure 1. *Coordinate axes and angular conventions.*

The incident wave vector, with wavelength λ, is determined in the coordinate system by the following expression:

$$\vec{k} = \frac{2\pi}{\lambda}(sin\theta cos\phi, sin\theta sin\phi, cos\theta) \qquad (1)$$

2.2. Radar cross section

RCS is a quantity representing the ability of a target to reflect electromagnetic energy when illuminated by radar waves. RCS depends on the target's size, shape, and construction material, as well as the frequency and incident angle of the incoming wave [10, 14, 15]. RCS is denoted as σ and defined by the equation:

$$\sigma = \lim_{R\to\infty} 4\pi R^2 \frac{|E_s|^2}{|E_i|^2} \qquad (2)$$

where: E_s is the scattered electric field amplitude, E_i is the incident electric field amplitude, and R is the distance from the target to the radar.

The unit of RCS is square meters (m^2), or expressed in decibels relative to a square meter (dBsm): $\sigma_{dBsm} = 10\log_{10}(\sigma)$. The incident plane wave electric field intensity is determined by:

$$E_i = E_0 e^{-j\vec{k}\cdot\vec{r}} \qquad (3)$$

where ***r*** is the position vector of the UAV. Anti-drone radar systems are designed to detect targets with very small RCS, often smaller than 0.1 m^2 [11, 16, 17].

2.3. Physical optics method

PO is a high-frequency approximation method based on Huygens' principle and the surface equivalence principle. The application of the PO method in this study relies on several fundamental assumptions: the target acts as a perfect electrical conductor (PEC) [12, 13], the observation is strictly under far-field conditions, the target dimensions are significantly larger than the operating wavelength, and the effects of wave polarization are ignored. On an ideal conductive surface, the surface current density is:

$$\mathbf{J}_s = 2\hat{n} \times \mathbf{H}_i$$

where $\mathbf{H}_i$ is the incident magnetic field and $\hat{n}$ is the unit normal vector, $\boldsymbol{H_i} = \frac{1}{\eta}\hat{k} \times \boldsymbol{E_i}$.

For 3D objects, the current density is only considered for the illuminated surface: $\hat{n} \cdot \hat{k} < 0$ for shadowed regions. The magnetic vector potential is:

$$\mathbf{A}(\mathbf{r}) = \frac{\mu}{4\pi}\int_S \mathbf{J}_S(\mathbf{r}')\frac{e^{-jkR}}{R}dS' \tag{4}$$

where: μ - Permeability of the environment; ***r*** - Observation point position; ***r'*** - Position on the surface; *S* is the scattering surface area. For the far-field:

$$R \approx r - r'$$
$$\frac{e^{-jkR}}{R} \approx \frac{e^{-jkr}}{r}e^{jk\cdot r'} \tag{5}$$

Then the far-field scattered electric field is determined as:

$$\mathbf{E}_\mathbf{s}(\mathbf{r}) = j\omega\mu\frac{e^{-jkr}}{4\pi r}\left[\hat{r}\times\left(\hat{r}\times\int_S \mathbf{J}_S(\mathbf{r}')e^{jkr\cdot\mathbf{r}'}dS'\right)\right] \tag{6}$$

Substituting expressions (3) and (6) into expression (2) and simplifying for the monostatic case, the monostatic RCS expression takes the form:

$$\sigma(\theta,\phi) = \frac{k^2}{4\pi}\left|\int_S (\hat{n}\times\vec{H}_i)e^{-jk\hat{r}\cdot r'}dS\right|^2 \tag{7}$$

For a given 3D UAV model discretized into *N* triangular mesh elements, the modified monostatic RCS determination expression is

$$\sigma(\theta,\phi) = \frac{k^2}{4\pi}\left|\sum_{i=1}^{N}(\hat{n}_i\times\vec{H}_i)A_i e^{-jk\hat{r}\cdot r_i}\right|^2 \tag{8}$$

where: A_i is the area of triangle *i*, $\hat{n}_i$ - Unit normal, $\mathbf{r}_i$ - Geometric center.

In this study, the hypothetical radar system operates in the range of 8.7 ÷ 9.65 GHz (corresponding to X-band). For the numerical simulations and results presented in Section 3, a specific operating frequency of f = 9.0 GHz (with a corresponding wavelength λ ≈ 0.033 m) was selected to represent typical X-band characteristics.

3. RESULTS AND DISCUSSION

3.1. UAV model and calculation condition

The CX24v1 UAV was designed in 3D (Figure 2) by the authors; aerodynamic and structural calculations, and successful experimental manufacturing were conducted to serve as a target drone with variable wing shape features. It is suitable for training anti-UAV anti-aircraft artillery, radar systems, cameras, and missile seekers. The CX24v1 has a wingspan varying from 1.4 ÷ 2 m, a maximum speed of 125 km/h, a cruise speed of 80 km/h, and an endurance of 30 minutes.

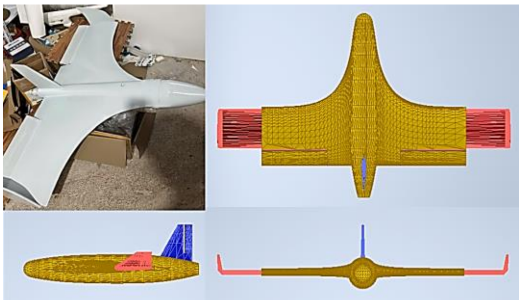

Figure 2. *3D model and the CX24v1 UAV.*

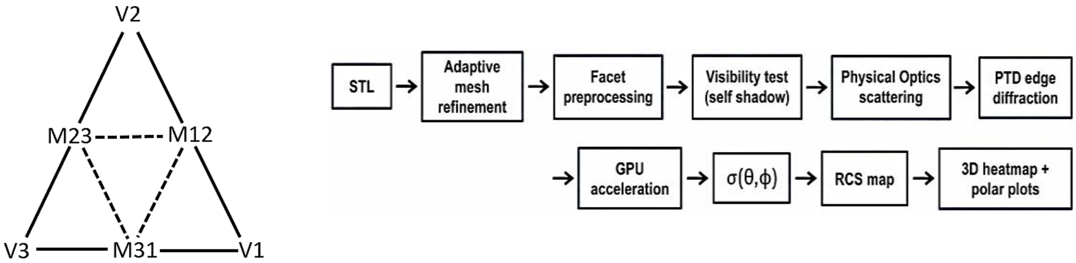

a) Mesh refinement scheme. *b) Algorithm flowchart for RCS determination.*

Figure 3. *Calculation diagrams of PO.*

The radar elevation angle θ varies in the range from 0° to 180° with a 1° step. The azimuth angle φ scans from 0° to 360° counter-clockwise with a 1° step. The triangular mesh for the CX24v1 model was automatically generated using the Mesh module of Ansys Workbench with 23,458 triangular facets (Figure 2). A triangular mesh element is called a facet.

With coarse meshing, facets have uneven sizes; facets with large areas will, according to the reflection principles of the PO method, create very large RCS peaks that do not match reality. Therefore, in this study, to increase accuracy, facets with $L_{facet} > \lambda/8$ are subdivided into 4 smaller facets. This refinement process completes only when all facets satisfy the condition $L_{facet} \le \lambda/8$ (Figure 3a). After refinement, the number of facets for the CX24v1 model is 93,832.

The calculation program was built in MATLAB based on the PO RCS expressions in Section 2 and on Figure 3b.

3.2. Results and discussion

3.2.1. Model verification

The study verified the calculation model with a 1 × 1 m² metal plate. The radar wave illuminates the vertical longitudinal plane (φ = 0°), with θ scanning from 0° to 90°. For a 1 m² flat metal plate, theoretically [11, 14]:

$$\sigma(\theta) = \frac{4\pi A^2}{\lambda^2} \cdot \cos^2(\theta) \cdot \left[\frac{\sin\left(\dfrac{kL}{2}\sin\theta\right)}{\dfrac{kL}{2}\sin\theta} \right]^2 \qquad (9)$$

The results shown in Figure 4 demonstrate that as the number of facets on the plate surface increases, the PO calculation results converge significantly toward the theoretical curve. At N = 10 facets, there is a clear deviation from the analytical solution, especially at off-normal angles.

However, when the mesh is refined to N = 80 facets, the curve almost perfectly overlaps with the theoretical data. This confirms that the self-developed PO program provides highly reliable results, establishing a solid scientific foundation for analyzing complex geometries like the CX24v1 UAV.

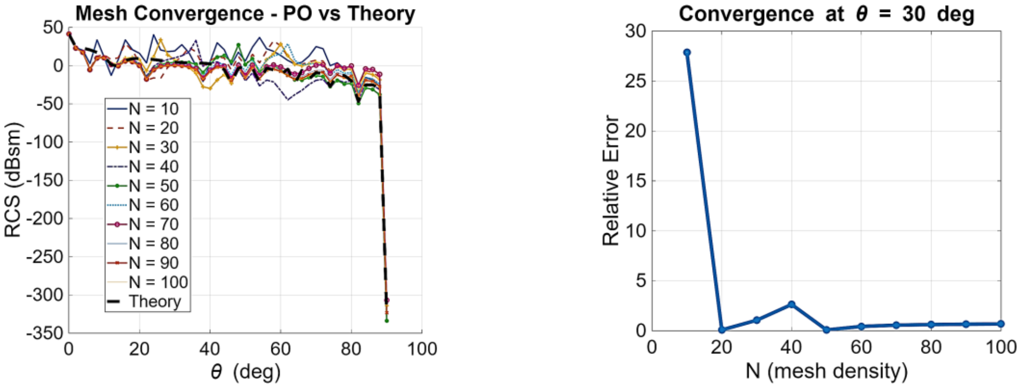

a) Calculation model verification of the RCS metal plate. *b) Mesh convergence check at θ = 30°.*

Figure 4. *Plots for mesh convergence check and calculation model verification.*

3.2.2. RCS calculation for CX24v1 UAV

RCS results for the CX24v1 are represented as polar plots for characteristic planes: vertical longitudinal (φ = 0°), vertical lateral (φ = 90°), and horizontal (θ = 90°).

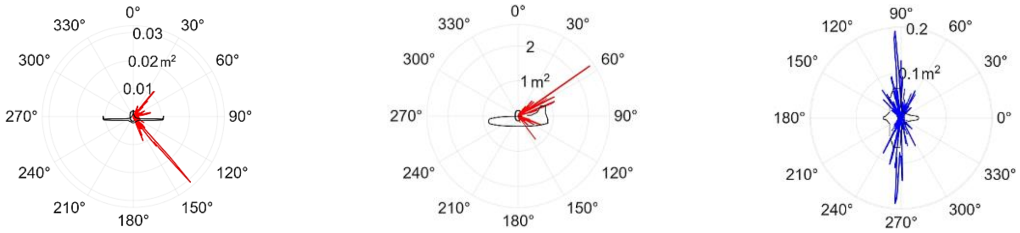

a) φ = 0° *b) φ = 90°* *c) θ = 90°*

Figure 5. *RCS polar plots (m^2) of CX24v1 UAV by projections.*

In the vertical longitudinal plane (Figure 5a), RCS values are relatively low, with the main reflection lobes concentrated at θ ≈ 45° and 135°, corresponding to the structural tilt of the fuselage and tail sections.

In the vertical lateral plane (Figure 5b), RCS increases sharply. The maximum peaks occur when the incident wave is nearly perpendicular to the wing surfaces (around θ≈ 60° and 120°), where the effective scattering area is maximized.

In the horizontal plane (Figure 5c), the UAV shows a minimum RCS at the nose (φ ≈ 0°), which is an advantage for stealth. However, the side-on RCS (φ ≈ 90° và 270°) is significantly larger due to the large vertical surface area of the fuselage and tail (φ ≈ 180°).

Figure 6 shows that RCS increases and remains relatively stable as φ increases. Peaks consistently appear near θ≈ 45 ° and 135 °. The variation of RCS as a function of the elevation angle θ across different azimuth planes φ reveals a consistent fluctuation pattern. The fluctuations are more intense at side-view angles (φ approaching 90 °), where the structural complexity of the wings and fuselage creates multiple reflection points.

Maximum and average RCS (Figure 7) are minimized at φ = 0° and increase as the plane rotates toward φ = 90° (side illumination). This figure compares the peak (Max) and average (Mean) RCS values. It is observed that the Mean RCS is consistently much lower than the Max RCS, indicating that the strong reflections are highly directional and limited to narrow angular sectors. The overall trend shows that the UAV is most visible to radar when viewed from the side.

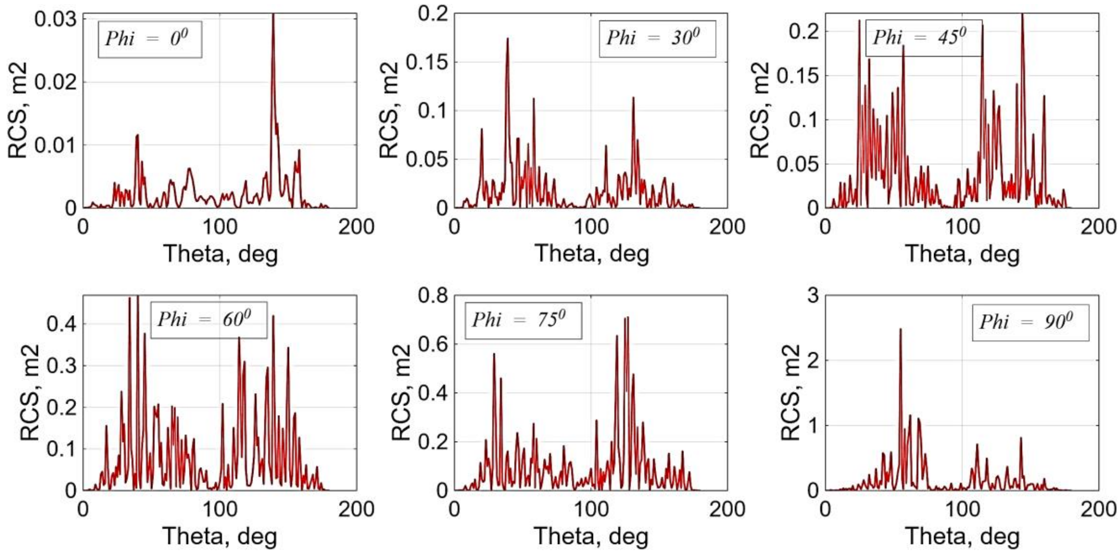

Figure 6. *RCS plots (m^2) of CX24v1 UAV vs. theta angle.*

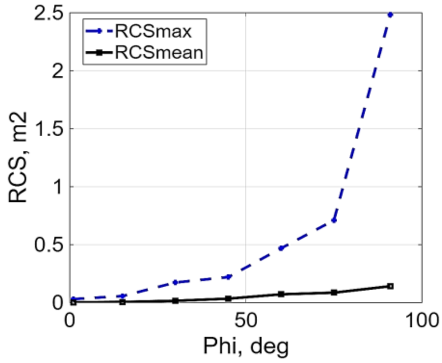

Figure 7. *Maximum and mean RCS of CX24v1 UAV at different φ planes.*

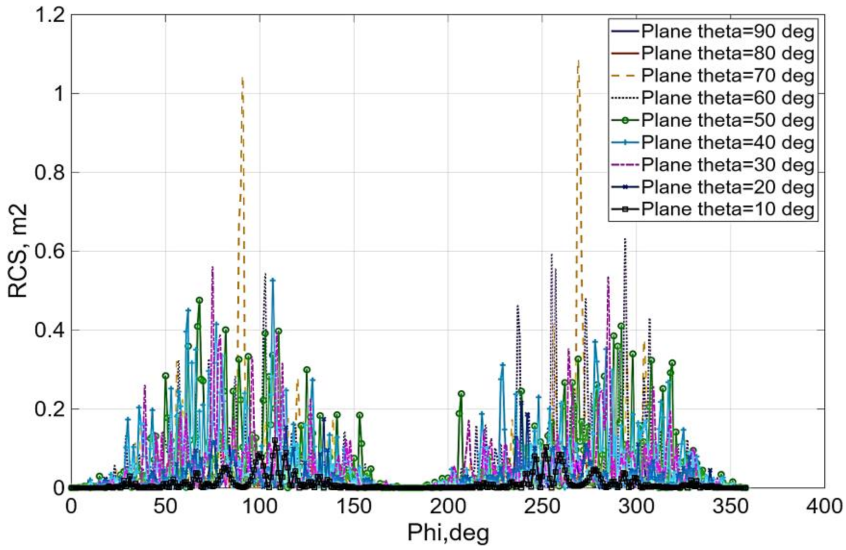

Figure 8. *RCS plots (m^2) of CX24v1 UAV vs. phi angle.*

In Figure 8, the RCS values across the full 360 ° azimuth range demonstrate the anisotropic nature of the UAV's scattering. Although the PO method does not account for complex phenomena like edge diffraction or multi-bounce scattering, these results provide a critical quantitative map of "hot spots" where the UAV is most vulnerable to detection.

RCS values range from 0.01 m^2 to several square meters. While PO does not fully describe edge diffraction or multi-order scattering, it allows for rapid calculation across a wide angular domain during preliminary design to optimize aerodynamic configurations for RCS reduction.

Discussion on target drone requirements: As a prototype target drone for surface-to-air artillery drills, the CX24v1 is expected to emulate the radar signature of typical small-scale threat UAVs. Literature suggests that such threats generally exhibit an RCS between 0.1 m^2 and 1 m^2 in the X-band. As demonstrated in the results (Figures 5-8), the average RCS of the CX24v1 falls well within this required range. The maximum peaks, while larger, are highly directional. Therefore, the calculation results confirm that the current aerodynamic shape fully satisfies the RCS requirements for realistic radar training scenarios.

4. CONCLUSIONS

The paper has successfully developed a computational model to determine the RCS of fixed-wing UAVs using the Physical Optics (PO) method combined with 3D triangular mesh discretization. Through the case study of the CX24v1 UAV, the research highlights that the RCS distribution is highly dependent on the illumination angle, with the nose-on aspect offering the lowest detectability. The parallelized algorithm implemented in MATLAB significantly improves computational efficiency (e.g., reducing the computation time for 93,832 facets over a full 3D angular sweep from approximately 2 hours in sequential mode to just 15 minutes using a 6-core processor), allowing for rapid assessment over a full spherical scanning domain. These findings provide a vital quantitative basis for predicting the detection range of anti-drone systems and serve as a technical reference for future studies on structural optimization and the application of radar-absorbing materials to enhance the stealth capabilities of domestic UAVs. Future work will focus on improving the current PO model by incorporating hybrid techniques (such as the Physical Theory of Diffraction or Equivalent Edge Currents) to address edge diffraction, to handle complex, non-flat surfaces with very small facets, and to evaluate the effects of non-metallic or radar-absorbing materials.

REFERENCES

[1]. P. Kardasz et al., "*Drones and possibilities of their use*", Journal of Civil and Environmental Engineering, Vol. 6, No. 3, pp. 1–7, (2016).

[2]. H. Rohling, "*18th International Radar Symposium (IRS)*", Cuvillier Verlag, (2017).

[3]. G. Wild, G. Murray and G. Baxter, "*Exploring civil drone accidents and incidents to help prevent potential air disasters*", Aerospace, Vol. 3, No. 22, (2016).

[4]. S. Shvetsova and A. Shvetsov, "*Safety when flying unmanned aerial vehicles at transport infrastructure facilities*", Transportation Research Procedia, Vol. 54, pp. 397–403, (2021).

[5]. M. Guo et al., "*Research on monostatic radar cross section simulation of small unmanned aerial vehicles*", Proceedings of the 2018 International Conference on Microwave and Millimeter Wave Technology (ICMMT), (2018).

[6]. M. Schneebeli et al., "*Drone detection with a multistatic C-band radar*", Proceedings of the 2021 21st International Radar Symposium (IRS), pp. 1–10, (2021).

[7]. M. Ezuma et al., "*Comparative analysis of radar cross-section-based UAV classification techniques*", arXiv preprint arXiv:2112.09774, (2021).

[8]. M. Ezuma et al., "*Radar cross section based statistical recognition of UAVs at microwave frequencies*", IEEE Transactions on Aerospace and Electronic Systems, Vol. 58, pp. 27–46, (2022).

[9]. K. C. Cai et al., "*Study on radar cross-section characteristics of quadrocopter group flight*", Proceedings of the 2021 International Symposium on Antennas and Propagation (ISAP), pp. 1–2, (2021).

[10].E. F. Knott, J. F. Shaeffer and M. T. Tuley, “*Radar cross-section*”, Aspects of Modern Radar, Artech House, pp. 444–448, (1988).
[11].C. A. Balanis, “*Antenna Theory: Analysis and Design*”, John Wiley & Sons, (2016).
[12].K. Kapoulas et al., “*Small fixed-wing UAV radar cross-section signature investigation and detection, and classification of distance estimation using realistic parameters of a commercial anti-drone system*”, Drones, Vol. 7, No. 1, p. 39, (2023).
[13].C. A. Balanis, “*Advanced Engineering Electromagnetics*”, John Wiley & Sons, (2012).
[14].E. F. Knott, J. F. Shaeffer and M. T. Tuley, “*Radar Cross-Section*”, SciTech Publishing, (2004).
[15].M. I. Skolnik, “*Radar handbook*”, IEEE Aerospace and Electronic Systems Magazine, Vol. 23, No. 5, p. 41, (2008).
[16].M. Pieraccini, L. Miccinesi and N. Rojhani, “*RCS measurements and ISAR images of small UAVs*”, IEEE Aerospace and Electronic Systems Magazine, Vol. 32, No. 9, pp. 28–32, (2017).
[17].P. Molchanov et al., “*Classification of small UAVs and birds by micro-Doppler signatures*”, International Journal of Microwave and Wireless Technologies, Vol. 6, No. 3–4, pp. 435–444, (2014).

TÓM TẮT

Ứng dụng phương pháp quang vật lý xác định diện tích phản xạ radar cho UAV cánh bằng

Bài báo trình bày nghiên cứu xây dựng mô hình tính toán diện tích phản xạ radar (Radar Cross Section – RCS) cho UAV cánh bằng dựa trên mô hình hình học ba chiều dạng lưới tam giác và phương pháp gần đúng Physical Optics (PO). Bài toán tán xạ đơn tĩnh được xây dựng dưới dạng tích phân bề mặt và được rời rạc hóa trên lưới tam giác của mô hình UAV. Thuật toán được tối ưu hóa bằng xử lý song song nhằm giảm thời gian tính toán cho toàn miền góc quét. Kết quả tính toán RCS theo mặt phẳng đứng và mặt phẳng ngang được biểu diễn dưới dạng đồ thị cực và được phân tích về đặc trưng phản xạ theo hướng. Kết quả cho thấy mô hình PO cho phép ước lượng nhanh phân bố RCS của UAV cánh bằng trong giai đoạn thiết kế sơ bộ.

Từ khóa: RCS; UAV cánh bằng; Physical Optics; Tán xạ điện từ; Mô hình số; Lưới tam giác.